REPORT DOCUMENTATION PAGE

Form Approved
OMB No. 0704-0188

1. REPORT DATE *(DD-MM-YYYY)*	**2. REPORT TYPE**	**3. DATES COVERED** *(From - To)*
26-04-2012	Technical Paper	

4. TITLE AND SUBTITLE

Development of Nonuniformities in Swirling, Rocket Injectors

5a. CONTRACT NUMBER

5b. GRANT NUMBER

5c. PROGRAM ELEMENT NUMBER

6. AUTHOR(S)
Malissa D.A. Lightfoot, Vinod Narayanan, Alan L. Kastengren, and
S. Alexander Schumaker

5d. PROJECT NUMBER

5f. WORK UNIT NUMBER
50260538

7. PERFORMING ORGANIZATION NAME(S) AND ADDRESS(ES)

Air Force Research Laboratory (AFMC)
AFRL/RZSA
10 E. Saturn Blvd.
Edwards AFB CA 93524-7680

8. PERFORMING ORGANIZATION REPORT NUMBER

9. SPONSORING / MONITORING AGENCY NAME(S) AND ADDRESS(ES)

Air Force Research Laboratory (AFMC)
AFRL/RZS
5 Pollux Drive
Edwards AFB CA 93524-7048

10. SPONSOR/MONITOR'S ACRONYM(S)

11. SPONSOR/MONITOR'S NUMBER(S)
AFRL-RZ-ED-TP-2012-098

12. DISTRIBUTION / AVAILABILITY STATEMENT

Approved for public release; distribution unlimited (PA #12265).

13. SUPPLEMENTARY NOTES
For presentation at the 24th Annual Conference on Liquid Atomization and Spray Systems (ILASS-Americas), San Antonio, TX, 20-23 May 2012.

14. ABSTRACT

A high-performing, stable rocket engine requires injectors which produce predictable, uniform, temporally stable sprays. The use of high-velocity gas to atomize a liquid, such as in an ox-rich engine cycle, can produce complex, unsteady behavior. Two types of unsteady behavior, pulsing and changes in the spray's centerline, were observed in a specific type of prefilming rocket injector—a Gas-Centered Swirl Coaxial (GCSC) injector. The reason for this unsteadiness is not well understood, and developing an improved understanding is complicated by the high optical density of the spray and its axisymmetric, swirling nature. Recent advances in image processing techniques through the use of Proper Orthogonal Decomposition (POD) and in time-resolved x-ray diagnostics are enabling additional information to be extracted from the spray and improving the understanding of spray instabilities. Here a series of geometries and operating conditions of GCSC injectors are examined with traditional image processing techniques to elucidate the basic nonuniform behavior of the spray and atomizing film. A single test condition is examined in detail using POD and time-resolved x-ray radiography. The results of these two techniques compare favorably with the traditional processing and complement the traditional approach by providing additional information. The POD analysis allows visualization of the location of unsteady structures, and the radiography provides details of the spray changes (i.e. changes in droplet size) during the unsteadiness.

15. SUBJECT TERMS

16. SECURITY CLASSIFICATION OF:			**17. LIMITATION OF ABSTRACT**	**18. NUMBER OF PAGES**	**19a. NAME OF RESPONSIBLE PERSON**
					Dr. Malissa D.A. Lightfoot
a. REPORT	**b. ABSTRACT**	**c. THIS PAGE**			**19b. TELEPHONE NUMBER** *(include area code)*
Unclassified	**Unclassified**	**Unclassified**	SAR	13	N/A

Development of Nonuniformities in Swirling, Rocket Injectors

Malissa D.A. Lightfoot[1*], Vinod Narayanan[2], Alan L. Kastengren[3], S. Alexander Schumaker[1], Stephen A. Danczyk[1]
[1]Air Force Research Laboratory, Edwards AFB, CA
[2]Oregon State University, Corvallis, OR
[3]Argonne National Laboratory, Argonne, IL

Abstract

A high-performing, stable rocket engine requires injectors which produce predictable, uniform, temporally stable sprays. The use of high-velocity gas to atomize a liquid, such as in an ox-rich engine cycle, can produce complex, unsteady behavior. Two types of unsteady behavior, pulsing and changes in the spray's centerline, were observed in a specific type of prefilming rocket injector—a Gas-Centered Swirl Coaxial (GCSC) injector. The reason for this unsteadiness is not well understood, and developing an improved understanding is complicated by the high optical density of the spray and its axisymmetric, swirling nature. Recent advances in image processing techniques through the use of Proper Orthogonal Decomposition (POD) and in time-resolved x-ray diagnostics are enabling additional information to be extracted from the spray and improving the understanding of spray instabilities. Here a series of geometries and operating conditions of GCSC injectors are examined with traditional image processing techniques to elucidate the basic nonuniform behavior of the spray and atomizing film. A single test condition is examined in detail using POD and time-resolved x-ray radiography. The results of these two techniques compare favorably with the traditional processing and complement the traditional approach by providing additional information. The POD analysis allows visualization of the location of unsteady structures, and the radiography provides details of the spray changes (i.e. changes in droplet size) during the unsteadiness.

[*]Corresponding author: malissa.lightfoot@edwards.af.mil

Introduction

In recent years the Air Force Research Laboratory has studied a specific type of prefilming atomizer for use in rocket engines, a Gas Centered Swirl Coaxial (GCSC) injector, in detail [1-3]. This injector utilizes a strong gas flow to atomize an annular liquid. The prior studies have shown that this type of injector exhibits a rich and complex behavior [3]. Several geometries and/or operating conditions produce unsteady sprays. To prevent confusion with combustion instabilities, a particular concern in rocket injectors, this unsteadiness is referred to as temporal nonuniformity or just nonuniformity. There were two main types of temporal variation identified in GCSC injectors. "Pulsing", a temporary increase in liquid mass in the spray, was observed typically through an increase in spray width. When the centerline of the spray varied with respect to the injector centerline then the behavior was termed "bouncing" [3]. These behaviors are, in general, undesirable but can be overcome by carefully choosing operating conditions and/or injector geometries. However, an understanding of the root cause of temporal behaviors, even at nonideal conditions, is sought to further the understanding of film atomization and GCSC injector operation.

The geometry and operating conditions of these injectors were originally motivated by a desire to produce stable combustion in a rocket engine [3, 4]. To accomplish this goal, a uniform spray which is independent of feedback from the combustion environment is essential. Because this is a prefilming atomizer, the atomization progresses from a wall-bounded film. Uniformity in the original film increases the likelihood of uniformity in the spray. A sheltered volume is provided for the entering liquid so that a complete film, as opposed to discrete wall-bound jets, can be formed prior to the liquid and gas coming into contact and the start of atomization. Without the shelter, discrete jets are clearly visible from ballistic imaging [5], and there is some evidence to suggest that the shelter is not necessarily effective despite fully filling prior to liquid-gas contact. The swirl and shelter should result in a flow which is uniform on the average, and that time-averaged uniformity is observed [4]. However, the lip initially separating the gas and liquid may introduce additional complexities leading to the observed time-dependent behavior. Lip geometry has been postulated as a cause for at least the pulsing type of spray nonuniformity observed in GCSC injectors.

Vorticity and, oftentimes, unstable or periodic motions are generated when a fast moving gas contacts a slow moving liquid [6]. The end of the separating lip has a finite thickness and this "step" will create a recirculation zone behind it. For certain step sizes this recirculation zone is unsteady [7]. The elimination of this step appeared to be a promising tactic for stabilizing the spray. However, investigations of sheets have indicated that an infinitely thin dividing boundary just upstream of the liquid-gas contact produces nearly infinite vorticity while a thicker divider produces substantially less vorticity [6]. Supporting evidence for the undesirability of thin lips has been observed in GCSC injectors: spray temporal nonuniformity is increased when the lip between the gas and liquid becomes nearly a knife edge [7]. Obviously, though, there is some optimal thickness as a very thick lip also appears to increase the temporal nonuniformity of a GCSC spray [3]. These observations are somewhat indirect: conclusions were drawn based on "by-eye" observations of the sprays and limited quantitative comparisons of spray width as a function of time from shadowgraphy of the spray.

The mechanism(s) by which periodic behaviors are created in GCSC sprays has not yet been established. Computational results suggest that a recirculation zone is created due to gas separation at the end of the lip [7]. This low pressure zone fills with liquid. As the liquid fills in the area the step becomes less pronounced and becomes more of a gradual decline. The recirculation zone is also displaced. Once the zone is filled and the recirculation lessened, however, the configuration is unstable and the liquid within the zone is shed downstream. The process then repeats. (Figure 1 has an illustration of this cycle for a very poorly designed lip—one that promotes separation allowing easy visualization of the process.) These previous computations were axisymmetric, but the swirling nature of the flow and the retention of jet-like structures in the spray (as suggested by the ballistic imaging [5]) may result in localization of this behavior. If shedding is axisymmetric (or nearly so) pulsing would result;

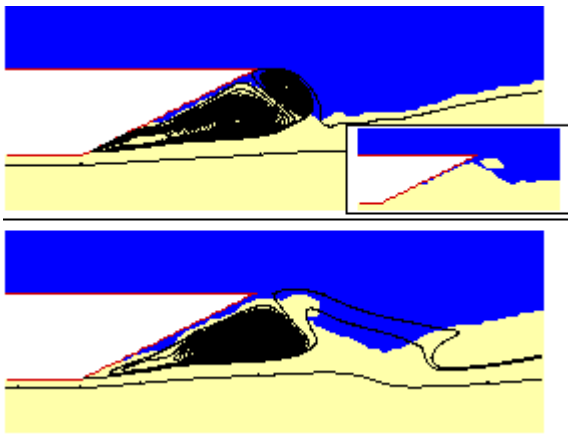

Figure 1: A close-up view of the lip (white) separating the liquid (blue) and gas (yellow) is shown along with select streamlines (black); flow is from left to right. Liquid is pulled up the step but a wave of fluid is produced when the gas-liquid interaction cause the recirculation zone to decay.

localization of the shedding could lead to a bouncing sort of behavior. Images from within the injector, near the separating lip, are available [2], but resolution, contrast and the transient nature of the flow make it difficult to confirm the CFD results. Additionally, the frequency of the shedding observed in the computations did not match with the experimentally observed pulsing [3, 7]. While the computational results provide some insight they are currently of limited utility, yet recent advances in image processing and experimental techniques allow the extraction of additional and more detailed information from experimental images. Additional data will help in verifying the hypothesized mechanism.

High optical densities and the axisymmetric nature of the injector prevent the use of many diagnostics and make the identification and tracking of individual spray and film features (e.g., surface waves, droplets) difficult or impossible. Typically, techniques which isolate frequencies in sprays have relied on tracking individual features [8-10]. Proper Orthogonal Decomposition (POD) has shown promise in overcoming this limitation. POD techniques have been extensively applied to a variety of fields over the past 15 years as a way to extract the most energetic modes of variability in the data being analyzed ([11-13], for example). Repetitive patterns that are not discernible by regular image processing can often be extracted from the information provided by and reconstruction of the data using the most energetic modes. POD has even been used in recent spray experiments to extract, using spectral analysis, the frequencies and wavelengths of importance in the atomization of a jet in cross flow [13]. However, in this work the main focus was on specific, localized structures which are not discernable in the current GCSC data.

Another relatively new technique, time-resolved x-ray radiography, shows promise in resolving the individual structures (i.e. droplets) within the spray. Because the main interaction of photons with the droplets is absorption instead of inelastic scattering, moderate-energy x-rays have benefits over visible light techniques in dense sprays. X-ray radiography has provided time-averaged mass distributions for many types of sprays [14-16]. Recent application of the technique for sprays with steady conditions has illustrated its ability to discern individual droplets above a threshold size, currently about 35 mm [17]. This technique, then, allows comparisons between the global information extracted from these dense sprays and the behavior of discrete objects within the spray.

A single geometry and operating condition that exhibits a strong periodic behavior is examined in detail here in order to improve the understanding of the process leading to periodic nonuniformity in GCSC sprays. The results available from spray shadowgraphy processed using a well-established but limited technique, image segregation, are compared to the results of processing the spray images with a Proper Orthogonal Decomposition (POD) technique. Additionally, images from within the atomizer cup are also analyzed using both traditional and POD techniques. POD helps to visualize the unsteadiness in both the cup and the spray as well as providing the frequency spectrum. Within the injector cup, only frequency spectrum from the traditional image processing techniques is available. Finally, time-resolved x-ray radiography is used to extract some additional information from various locations within the spray. The three methods of data analysis all give complementary information on the behavior of the injector and the development of the periodicity in the spray. They suggest that the periodicity does originate at the initial contact of the liquid and gas and persists from the lip through to the spray. This periodicity is shown to be the result of periods of few or small droplets followed by periods of several, large droplets. In the film, the behavior alternates sides—a bouncing behavior—but the spray evidence is less clearly bouncing.

Experimental Methods

Hardware

A Gas-Centered Swirl Coaxial (GCSC) injector is a type of prefilming atomizer. Liquid enters through four holes tangential to the injector cup creating a swirling film. The film is initially separated from the gas by a sheltering lip. This volume allows the film to develop prior to contact with the gas. Unswirled gas enters axially. The gas post has an L/D greater than 14 prior to contacting the liquid. An array of geometries and conditions were minimally assessed using traditional image processing techniques. A single geometry and operating condition was examined in detail using the three processing techniques. The details of this test case are given in Table 1; it is referred to as Case A throughout the test. The ranges of the other geometries and operating conditions examined only briefly are given in Table 2. A sketch of the injector is shown in Fig. 2.

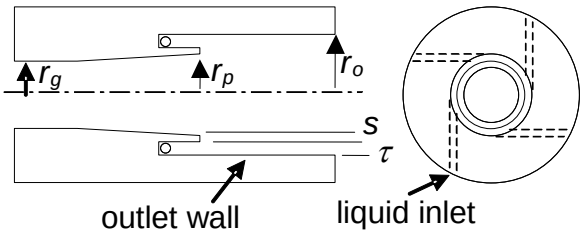

Figure 2: A schematic of a GCSC injector. Table 1 and 2 give the dimensions examined here. r_p is fixed at 6.35 mm.

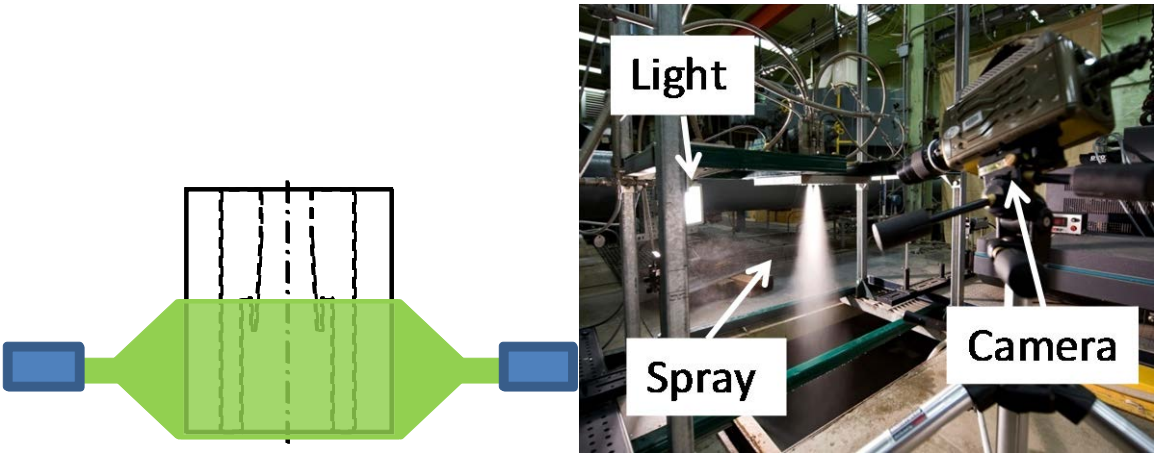

Figure 3: The laser-lighting for the film is shown as a simple cartoon (a). A photograph of the backlighting set-up for the spray imaging is also given (b).

Parameter	Value	Units
r_p	4.45	mm
r_o	7.62	mm
s	1.52	mm
τ	1.65	mm
m_g	0.036	g/s
m_l	0.043	g/s
Φ	44	

Table 1: The geometry and operating conditions for Case A including momentum flux ratio, Φ.

Parameter	Range	Units
r_p	3.43-9.27	mm
r_o	7.62-11.43	mm
s	0.178-3.43	mm
τ	1.32-1.98	mm
m_g	0.018-0.080	g/s
m_l	0.023-0.080	g/s
Φ	5-150	

Table 2: The full range of geometry and operating conditions considered are listed.

Water and nitrogen are used as simulants for the propellants that would be used in typical operation of the injector (liquid hydrocarbon and oxygen). Flow rates are controlled using metering orifices—sonic nozzles or cavitating venturis. The uncertainty in flow rates is estimated to be less than 4% for the gas and less than 1% for the liquid. The injector exits to the atmosphere. Tests were conducted at the Air Force Research Laboratory's "Flow Lab" and at Argonne National Laboratory's Advanced Photon Source (in the 7-BM beamline). The atmospheric pressure differs at the two locations: at AFRL it is typically 0.917 bar (13.3 psia) while at ANL it is typically 0.999 bar (14.5psia).

High speed video was obtained using a Vision Research Phantom v7.3 camera. Images were taken inside the injector cup and downstream of the injector body. Lighting for the in-cup video (video of the film) was provided by two variable-power, dpss lasers operating between 200 and 500 mW. The lasers were formed into sheets using two identical sets of optics. The sheets were diametrically opposed and located just off of the centerline of the injector body. The 1 to 2 mm off-axis orientation improves the amount of light collected by the camera and, therefore, the contrast of the images. There is some distortion of the film thickness due to this positioning, so the thickness cannot be quantitatively determined. The camera is located perpendicular to the light sheets (Fig. 3a). The downstream video (the video of the spray) is backlit using a halogen flood light with an acrylic diffuser (Fig. 3b). All video was acquired at a framing rate of 6006 frames per second. The exposure time for the in-cup video was 110 μs. More light is obtained in the backlit configuration allowing a much shorter exposure time of 3 μs.

The x-rays used in this study were created by a bending magnet at Argonne National Laboratory's Advanced Photon Source. The beam is conditioned and focused to create a 10keV beam with a FWHM of 5 x 6 μm. Time-resolved x-ray radiography data (the absorption of the spray) was obtained using a PIN diode. A titanium foil, utilizing the x-ray fluorescence from a thin sheet of titanium, was used to determine the baseline level of the x-rays prior to their entering the spray. More details on the set-up can be found in Ref. [17]. Data was taken at 1 mm increments across a 32 mm width of the spray. These transverse measurements were obtained 3 mm, 5 mm and 10 mm from the exit of the injector. Wetting of the injector face prevented measurements within 3 mm of the injector outlet. X-ray data were collected at a sampling rate of 1 MHz.

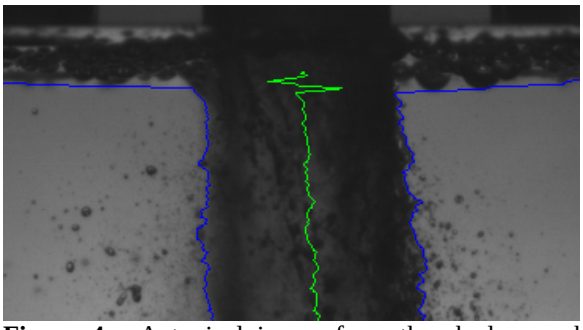

Figure 4: A typical image from the shadowgraphy with the spray boundaries and centerline, as determined by image segregation, shown.

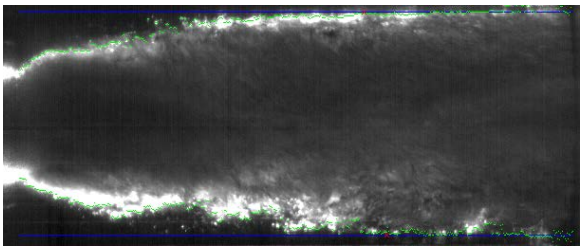

Figure 5: A typical image from inside the injector cup with the boundary determined from the automated process overlaid (green). The edges of the injector are shown by blue lines.

Data Processing

The spray shadowgraphs were processed using a simple image segmentation process (as described in Ref. [18]) as well as with a POD process. The POD is described below. For the traditional image processing, Otsu's method [19] was used to determine the threshold level separating the spray from the background. This threshold was then used to convert the 14-bit grayscale image to a black and white image. Matlab's *bwboundaries* routine was then used to trace the outline of the spray [20]. The outline is divided into a "left" and "right" boundary with a single location at every axial pixel. (Image resolution was 7.8 pixels per mm.) If the outline contains multiple points at an axial location then these are averaged together. The boundaries are used to calculate the width and centerline of the spray. Figure 4 shows a representative image along with the generated boundaries and centerline. Several downstream distances were selected—3 mm, 5 mm, 10 mm and 20 mm—to examine the periodicity of the spray. An fft was taken of the location of each boundary, the centerline and the spray width at each of these downstream locations. 5000 frames of video were analyzed. As a result, the frequency resolution is 1.2 Hz. Only a selection of the conditions listed in Table 2 were assessed using these processes.

The film video was also processed in two ways—the POD method described below and a method seeking to locate the film boundary based on changes in intensity. The boundary between the film and the gas is always indicated by a sudden transition from bright to dark. A typical image from the cup along with the located boundary is given as Fig. 5. Changes in film thickness, droplet dynamics within the core gas flow and other complexities produce a nonuniform intensity (brightness) along the injector's axis. As a result, a simple image segregation method cannot be used. Instead, the variation in intensity along a line perpendicular to the injector axis is examined from the gas core to the film. From the edge of the injector to its center the brightness changes slowly then sharply increases before decreasing again. The edge of the film is located within the run of increasing brightness with the precise location indicated by the two pixels with the steepest change between them. In well-lit, well-behaved films the location determined by eye from multiple users is within 2 pixels of the location found with the Matlab routine. (Two pixels is 0.13 mm.) However, in areas with less contrast or greater variation the user-to-user difference and the user-to-computer difference in boundary selection can be substantially larger. As a result, uncertainty is difficult to determine. However, large departures and seemingly erroneous values found by the automated routine are generally limited to single pixels or small runs of pixels. As with the spray images, an fft is performed on the boundary location at several axial locations (0.32 mm from the initial liquid-gas contact, 1.3 mm thereafter for 6.5 mm then 2.54 mm apart for another 25.4 mm with the last ~6.5 mm not examined because that is well beyond maximum length of the film). Here, as with the spray video, 5000 images are considered leading to a resolution of 1.2 Hz. In addition to the film height, a film length was determined and processed using an fft. The entire range of injector geometries and operating conditions given in Table 2 were examined using these procedures.

The POD is the same for both the film and spray videos. However, only Case A was analyzed using POD. The decomposition is performed using singular value decomposition in a scheme described in Ref. [18]. This decomposition results in eigenvectors which are uncorrelated in space and expansion (amplitude-time) coefficients which are uncorrelated in time. Eigenvectors are ordered with the most energetic mode being the first mode. Frequency information can be obtained from the expansion coefficients which are calculated as a projection of the data matrix onto the eigenvectors [18]. The current work differs from prior application of POD to GCSC injectors [18] in that before the decomposition the average is subtracted from each frame of video. Hence, only the fluctuating component of the spray is considered. The average is

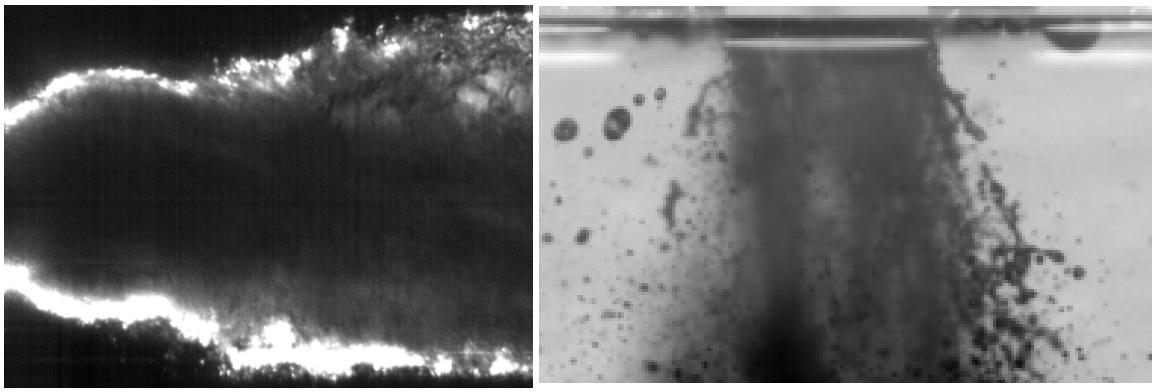

(a) (b)

Figure 6: Fields of view considered in the POD analysis (a) within the injector (244x388 pixels) and (b) in the near-field spray (421x265 pixels).

determined from the frames used in the POD analysis (typically in excess of 1400 frames). POD is memory intensive, so a limited field of view is considered. For the POD within the injector, the image was cropped to a size of 244 (across the injector) by 388 (along the injector) pixels (15.84 x 25.19 mm), corresponding to a field of view that started at the liquid-gas contact and extended to the approximate length of the film, i.e. approximately where the gas core contacted the injector walls (Fig. 6a). Only the first two thousand frames were selected for analysis to reduce computational expense. The resulting resolution of the frequency space is 3 Hz. Outside the injector, for the near-field spray characterization using POD, a field of view consisting of 421 (across the spray) by 265 (along the spray) pixels (53.97 x 33.97 mm) was chosen, as shown in Fig. 6b. With this larger field of view, POD could only be performed on 1400 consecutive frames from the movie, resulting in a resolution of 4.3 Hz.

The time-resolved x-ray radiography data was converted into a path length of water within the line-of-sight of the beam using Beer's Law. The values recorded from the PIN diode were normalized by the values from the titanium foil. A baseline value was then determined by averaging the largest 1% of transmission values. The result was then converted to a path length of water using the absorption coefficient for water [21]. While individual droplet diameters and velocities can be approximated from these data [17], the current work focuses on extracting information about the periodic behavior of the spray. As a result, an fft was performed on just over 1 million (2^{20}) data points and single periods of the data were compared at several locations within the spray. The frequency resolution is ~1 Hz for the analysis of these data. A typical time series is shown in Fig. 7. As with the POD, x-ray radiography was only applied to Case A.

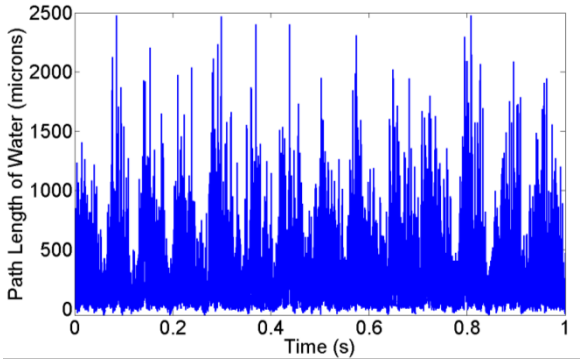

Figure 7: The path length of water in the x-ray beam as a function of time over a 1 second period.

Results and Discussion

Initial comparisons of the film behavior and the spray behavior were made using the unprocessed video of the cup and real-time, "by-eye" observations of the spray. The entire range listed in Table 2 was assessed. From these observations a clear unsteadiness was observed in both the film and the spray at many operating conditions. Whether this unsteadiness was periodic or random, the level of unsteadiness and any relation between the film and spray observations were not determinable from these first investigations. Over one hundred cases were examined in this way and several geometries and conditions produced an array of unsteady behaviors. (A selection of cases and a more detailed description of nonuniformites can be found in Ref. [3].) Case A (Table 1) was selected for additional focus, in part, because the unsteadiness was very visible and appeared periodic in this rough assessment.

Having qualitatively established the existence of temporal nonuniformity, the film video was processed using the traditional image-processing technique described above. Numerous injector geometries and conditions were again assessed, and the majority of them had a dominant frequency in the variation of film

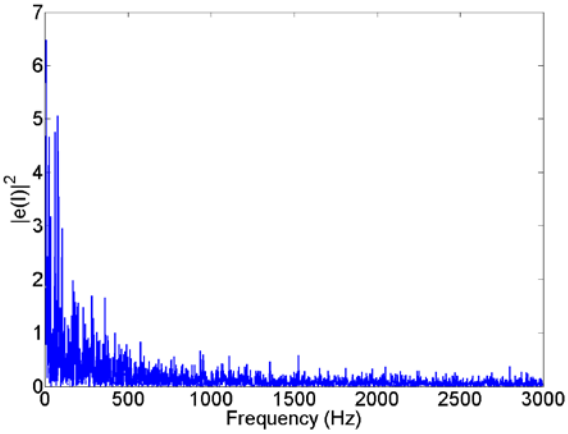

Figure 8: Spectral energy plot from traditional image processing of the film length for a typical case with no dominant frequency.

height at one or more axial locations or in the variation of length of the film. Often, however, this frequency was either localized to a single position or inconsistent in the axial direction (or from one observed side of the film to the other). Some of the inconsistencies likely stem from noise in the images resulting in difficulties and errors in determining the film boundary. However, some types of nonuniformities could result from localized disturbances [3] which would be observed as periodicity in only limited areas of the film. For example, asymmetric pulsing events were observed and these are often accompanied by waves which are visible only on a single side of the film. Consequently, that single side may be the only one which contains periodic behavior and in which a dominant frequency could be measured. There is some expectation, then, that the location(s) where films exhibit dominant frequencies provides information about the expected types of spray nonuniformities.

In the range of cases examined, the dominant frequency of the film did not exceed 350 Hz and, in general, frequencies were in the range of 8 to 100 Hz. The spectral power of the peak frequency was lower if the dominant frequency was higher than 100 Hz compared to the spectral power of dominant frequencies below this value. There is a general cascade of energy from low frequencies to higher frequencies as shown in Fig. 8. In Case A the film had a dominant frequency of 16.82 Hz observed at multiple axial locations and on both sides of the film. Figure 9 contains a spectral energy plot of this case.

The POD technique finds similar frequencies when applied to the film in Case A. The frequency associated with the largest expansion coefficient is 20 Hz as seen in Fig. 10. The other expansion coefficients contain additional peaks of lesser power. Of particular interest is the low-power peak at 880 Hz. This peak is interesting because it occurs in several of the expansion

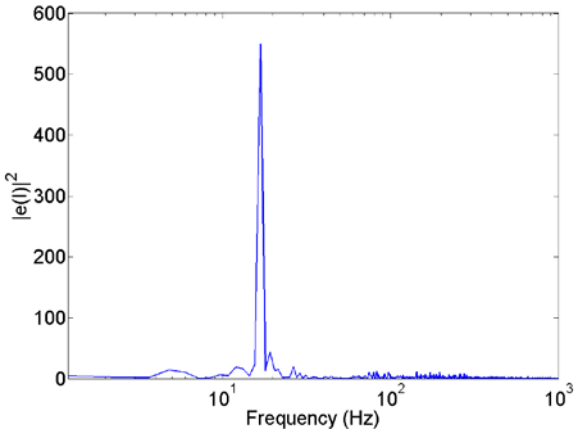

Figure 9: Spectral energy from traditional image processing of the film in Case A shows a dominant frequency in film length variation at 17 Hz. Unlike the POD results (Fig. 10) there is no signature at 880Hz.

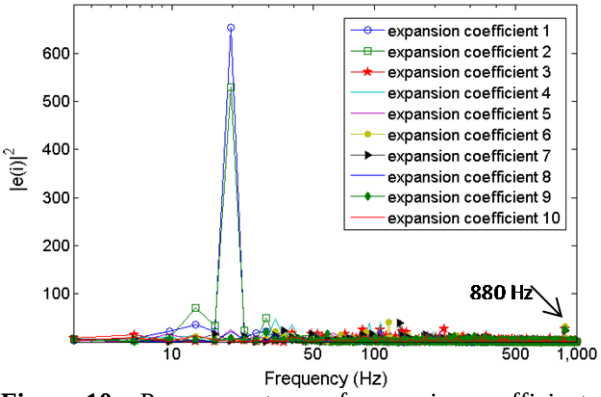

Figure 10: Power spectrum of expansion coefficients of the first 10 modes from the POD analysis. There is a dominant frequency in modes 1 and 2 at ~20 Hz. There are several different peaks in the range of 100-200 Hz for various modes. Modes 3, 7 and 9 (solid symbols) all have a peak at 880 Hz.

coefficients (see solid symbols in Fig. 10); the only other frequency occurring in multiple expansion coefficients is the dominant 20 Hz frequency. The traditional image processing technique did not find any peaks in this location (inset of Fig. 9). Frequencies in the range of 880 Hz are more troubling in terms of combustion stability and feedback than relatively low frequencies around 20 Hz. As a result, the current, traditional processing does not appear to be ideal for frequency assessments of these rocket injectors.

Both processing techniques produce additional information beyond the determination of frequency content in the film. The phase angle, or its relative difference, can be seen in graphs of film height at a specific downstream location over time (Fig. 11). The relative angle between the top and bottom films provides some indication of whether the nonuniformity

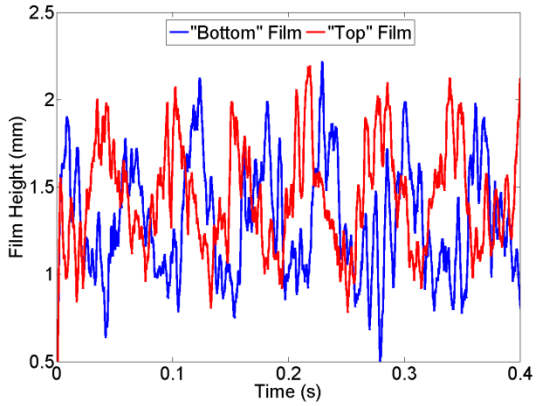

Figure 11: The film height as a function of time (at 9.4 mm) clearly shows a phase lag between the sides of the film.

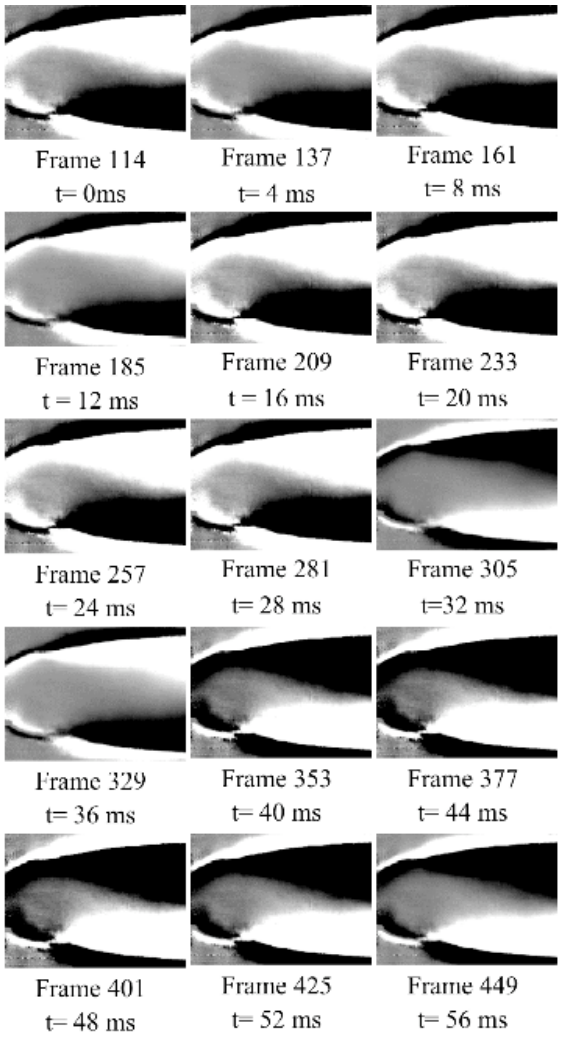

Figure 12: Reconstructions from mode 1 of the POD analysis of the film, shown here at an interval of 41.6 ms, shows approximately 20 Hz low frequency change in intensity between the top and bottom mixing layers.

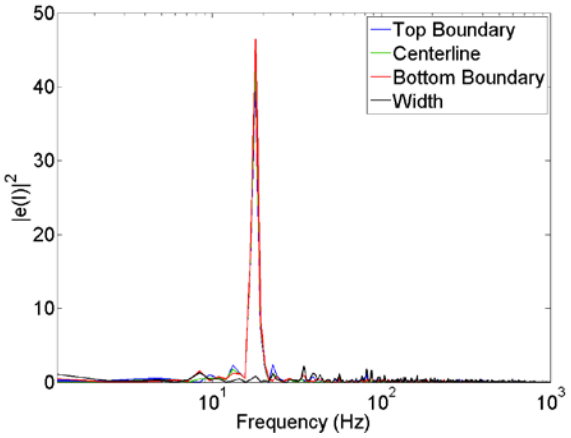

Figure 13: The spectral energy plot for the spray in Case A shows a dominant frequency at 18.02 Hz in all examined parameters except the width. These results are at 5 mm from the injectors exist using image segmentation.

is axi- or a- symmetric. In Case A, as illustrated in Fig. 11, the nonuniformity is asymmetric with a phase lag in the vicinity of 125°. Meanwhile, as applied (i.e. with the averaged image subtracted) the POD technique allows the origination and propagation of unsteady structures, if they exist, to be visualized. Figure 12 shows an example time series of POD fluctuating intensity reconstructions of mode 1. The corresponding power spectrum for the amplitude coefficients of this mode, represented by the blue open circles in Fig. 10, indicates a strong peak in the power spectrum at 20 Hz. The reconstructions in Fig. 12 indicate that the dominant frequency of this mode corresponds to changes in intensity from white to black between the upper and lower mixing layers. Since the POD is performed on fluctuations in intensity after subtracting the mean intensity, the reconstructions in Fig. 12 can be interpreted as a low frequency "flapping" of the mixing layer where atomization is occurring within the injector. Similar reconstructions of higher modes can reveal the cause of the lower powered, higher frequency peaks in the power spectrum in Fig. 10, but have not yet been completed. The flapping and origination point of the variation—at or very near the beginning of the field of view—lend support to the idea that film nonuniformities result from the interaction of the gas and liquid at its initial contact point.

The structures observed in the film through POD processing appear to remain intact to and past the exit of the injector. A small subset of sprays was quantitatively examined through image segmentation of the shadowgraphs to assess if structures existing in the film translated into periodicity within the spray. The chosen sprays all had self-consistent, dominant frequencies at multiple locations within the film when processed using traditional techniques. As with the

traditional imaging processing of the film, the image segmentation results from these spray show a general cascade of energy from the low frequencies and very little spectral energy above a few hundred (200-400) Hz. When dominant frequencies exist in both the film and the spray, the frequencies are equal within the resolution of the measurements. However, there are a few cases, typically for higher frequencies in the film, where no dominant frequency is observed in the spray despite a clear frequency in the film. Overall, the film nonuniformity does appear to translate into spray behaviors in most cases; yet, higher frequency behavior is not measured in the spray. Because the film chosen for further investigation (Case A) had a relatively low frequency (Fig. 13), it is unclear if higher frequencies are attenuated during the evolution and expansion of the spray or if there is a limitation in the shadowgraphy-image segmentation technique.

Dominant frequencies were sometimes present in all four of the spray parameters examined from the shadowgraphy (width, centerline and both sides of the spray). In other instances periodicities were only observed in one or more parameters. Typically, dominant frequencies would exist in the boundaries and the centerline but not the width or vice versa. A periodic width variation would represent a pulsing behavior while a periodic variation in all parameters except the width would represent a bouncing behavior, i.e. a behavior where the centerline of the spray varies with respect to the centerline of the injector. Case A does not have a dominant frequency in the width (Fig. 13), although there are peaks at 18.02 Hz (the dominant frequency in the other parameters) and 34.8 (within the uncertainty that is twice the dominant frequency in the other parameters). The lack of width variation coupled with the asymmetric film variation would suggest a bouncing type of behavior. Comparing the temporal behavior of the four measured spray parameters provides additional information as to the character of the nonuniformity. Further evidence that Case A is bouncing is reflected in the lack of phase offset between the spray's boundaries (Fig. 14). If the spray was pulsing, the two boundaries would be expected to be nearly 180° out of phase or nearly so (some offset due to the swirling nature of the film could occur). In-phase motion would translate to the movement of the spray's centerline, which is also reflected in the temporal behavior shown in Fig. 14.

The POD analysis also provides additional information on the character of the nonuniformity. Figure 15 shows the mode 1 time series reconstructions of the near-field spray. As mentioned before, the mean intensity of the time series was subtracted prior to POD analysis. Hence these images indicate spatial changes in intensity fluctuations with time. Consistent with the low frequency flapping seen in the injector (Fig. 12), the

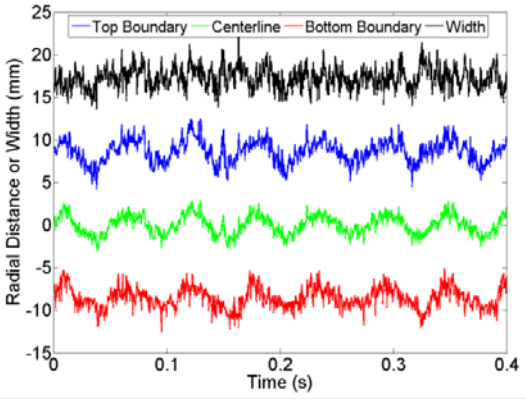

Figure 14: The temporal behavior of Case A indicates a strong periodicity in the edges of centerline of the spray but no organized motion in the width. The behavior 5 mm from the injector exit is shown here.

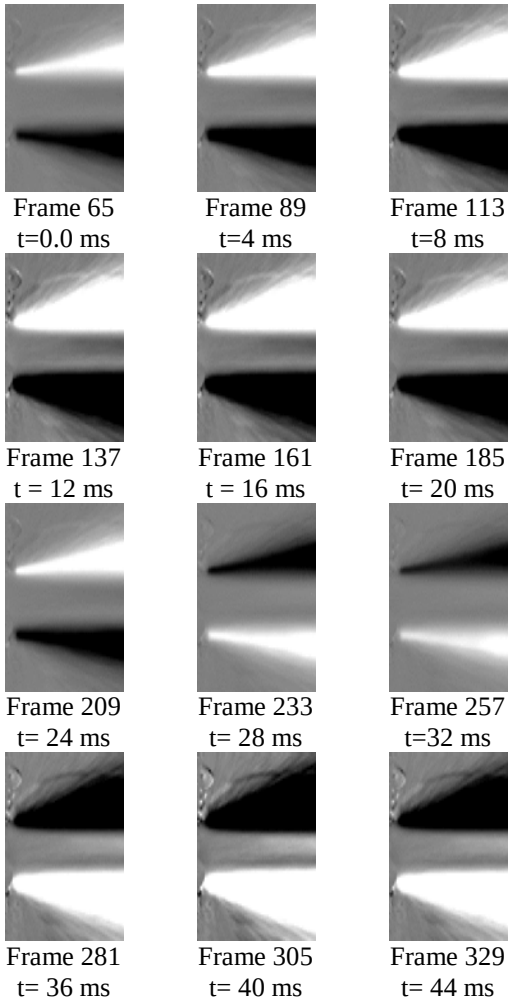

Figure 15: Time series reconstructions of mode 1 of the near-field spray. The POD was performed after subtracting the mean intensity. This mode captures low frequency in the spray which is consistent with the low frequency behavior in the injector as shown in Fig. 12.

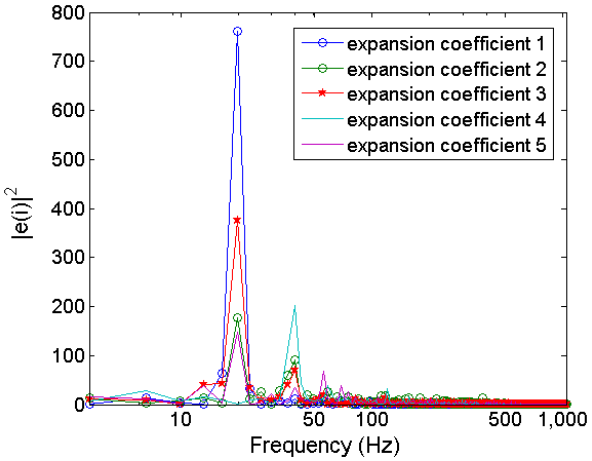

Figure 16: The POD analysis of the spray shows a clear dominant frequency at 20 Hz in modes 1-3, but no evidence of the 880 Hz signal in the first 5 modes.

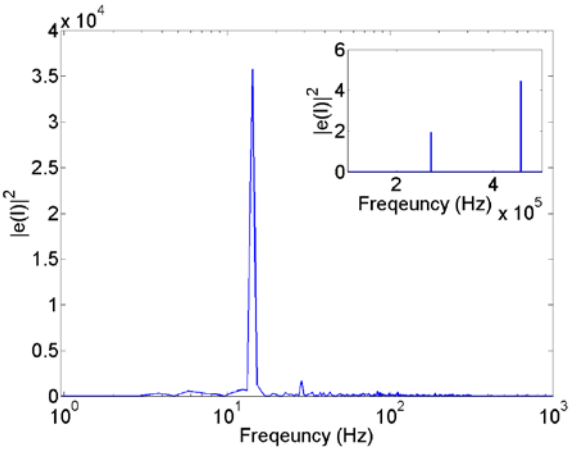

Figure 17: A dominant frequency in the range of 14.3 Hz exists in the x-ray radiography data. There are also several peaks at very high frequency as a result of the x-ray generation process shown in the inset.

mode 1 reconstruction of the spray indicate a low-frequency change in the spray's centerline (bouncing). From Figs. 12 and 15, it can be concluded that the flapping of the mixing layers within the injector causes the spray's bouncing behavior. The structures in Fig. 15 clearly show an increasing then decreasing departure from the centerline followed by a change in "direction". This type of behavior is echoed in the unsteady boundary movement shown in Fig. 14. The unsteady structures are only observed on the periphery of the spray. The bouncing nature of the spray would generally lead to more energy in these structures. However, the lack of observed structure near the sprays centerline may result from the optical density and shadowgraphic nature of the images which may present resolution of internal structures; additionally, the reconstruction in Fig. 16 is of the first mode, where the predominant unsteadiness is the bouncing.

Figure 16 shows the power spectrum of exapnsion coefficients from the first five modes of the POD analysis. The first three modes show strong peaks at 20 Hz, indicative of the bouncing observed in Figs. 14 and 15. This frequency is consistent with the flapping frequency of the mixing layer within the injector (Fig. 10). These POD results also suggests that high frequency components of the atomization process may be degraded and "washed out" in spray evolution and expansion. The POD analysis of the film images had several modes with peaks around 880 Hz, but the analysis of the spray images does not show any peaks at or near 880 Hz (Fig. 16). As with the shadowgraphy, only relatively low frequencies appear to have significant energy in the spray. The lack of higher frequencies is still not completely proven, however, since the optical density and lack of ability to resolve individual components and/or the central core of the spray may prevent the technique from measuring these frequencies.

The time-resolved x-ray radiography, which does resolve individual components, supports the image analysis results. A clear periodic behavior can be seen in the time trace (Fig. 7) at some locations in the spray. Analysis of the signal through fft shows that the dominant frequency is in the range of 12.4 to 15.4 Hz, varying with measurement location. The most common value is 14.31 Hz. The variation in dominant frequency does not appear to be systematic with axial or transverse location and, so, likely represents the uncertainty associated with the analysis. Outside of the spray and in the center of the spray, there were no dominant frequencies observed. Further, frequency peaks in the range of 880 Hz were not observed at any location. This result coupled with the POD result suggests that this higher frequency signal is "washed out" in the atomization and mixing through the end of the cup and downstream. It should be remembered that the 880 Hz signal is generally weaker than the one in the 15 Hz range, so the lack of long-distance propagation is not necessarily surprising. Further, the current x-ray results are limited in the velocity of droplets which can be resolved [17], so fast-moving core droplets are likely not being measured. In all of the points examined with x-ray radiography, even those outside of the spray, several very high frequency peaks exist (Fig. 17). These have less energy than the lower frequency peaks and are an artifact of the synchrotron and the generation of x-rays. The 271 kHz frequency, for example, represents the transit time of an electron packet around the ring.

The spectral energy in the dominant peak variously increases and decreases as the measurement location moves across the spray (Fig. 18). At all downstream distances examined the centerline of the spray does not

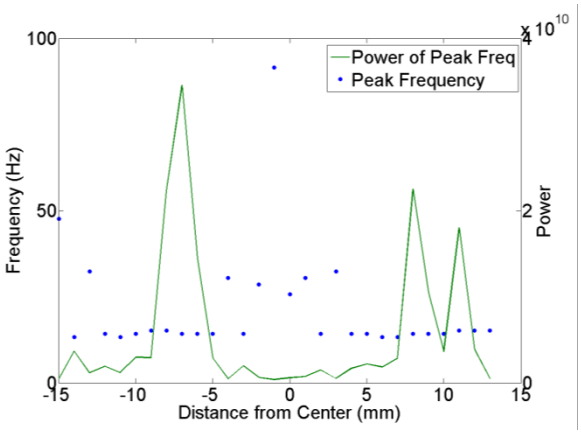

Figure 18: The spectral energy at the peak frequency and that peak frequency varies with location. The shown measurements were made 5 mm downstream of the injector exist. Not shown is the variation in relative dominance of the peaks.

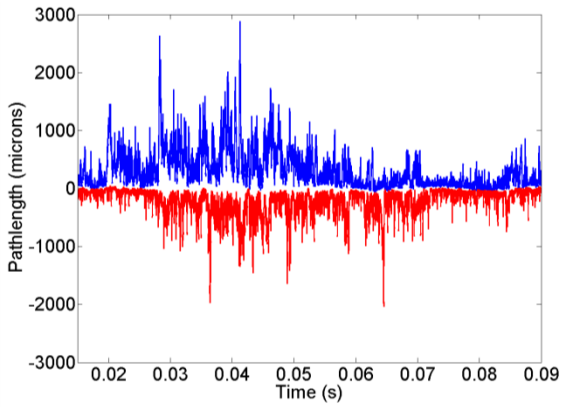

Figure 19: The time-resolved path length of water in the x-ray beam over a single period for locations 5 mm (blue) and 9 mm (red) to the left and right of the centerline. The red data are the negative of the path length to better highlight differences. Data is from 10 mm downstream of the injector outlet.

exhibit a dominant periodic behavior. A peak frequency is given in Fig. 18, but this frequency is not dominant as its power is similar to that of other peaks in the spectrum, typically within 10%. The reasons for the lack of dominant frequency near the spray's center are likely two-fold. First, from the shadowgraphy, the spray is bouncing, that is moving back and forth about the centerline. In similar sprays, the time-averaged mass distribution was nearly Gaussian in profile [4]. Small deviations near the center of the Gaussian profile produce little change in average mass, but small deviations near the edges of the profile have a much larger impact. Similarly, if the spray's centerline is moving and the measurements are near the center of the spray, where the majority of the mass is located, changes are likely to be smaller than if the measurement location is near the edge of the spray where substantially less mass is located. In other words, at some location in the center of the spray, the amount of mass (the size and number of the droplets) will not vary appreciably despite the bouncing. If the spray departs wildly from the centerline, this area will be very narrow and possibly not measurable, but if the spray centerline moves little, the majority of the spray may have undetectable changes. Of course, this interpretation is complicated because the spray is not moving in a plane perpendicular to the measurement volume, but the general idea still applies. The wider the area without a dominant frequency is, the smaller the departure from the injector's centerline. Another reason that the centerline may not have measurable periodicity is related to the line-of-sight nature of the x-ray measurement. Assume the spray is composed of an annulus, an "edge", and a core flow where the edge changes substantially with time while the core changes only slightly or not at all. At the extreme end of the spray the measurement line goes through only the edges of the spray, which are moving. When the measurement line is near the center of the spray it travels through two edges and the core of the flow and more total mass. Multiple droplets are more likely to be in the probe volume in the center of the spray and, consequently, more of them will be "steady". As a result, even though the measurement line travels through two varying edges, it may be more difficult to discern periodic behavior. In all by the center-most measurement of the spray, a strong peak does exist in the 12.5-14.5 Hz range even though this peak may not be the largest or dominant in the center region.

Beyond frequency information, the x-ray data provide additional details about the character of the periodic behavior. Figure 19 shows two time traces over what is approximately a single period (~0.07 seconds) at measurement locations with high spectral energy in the dominant frequency (at the edge of the spray). With the time series expanded, the periodicity is shown to consist of a span of few (or very small) droplets followed by a span of many, large droplets. Essentially, there are alternating periods of little or no mass followed by periods of relatively large amounts of liquid. Because the measurements at different locations in the spray are not acquired simultaneously, no phase shift information can be obtained and the exact type of behavior cannot be gleaned from the x-ray results. The behavior from one side of the spray centerline to the other is very similar (at the same transverse distance from the centerline). The behavior at various downstream locations is also similar.

Conclusions

The periodic nature of GCSC injectors at certain operating conditions has been examined using three

different methods. Film and spray images were evaluated using traditional, image segmentation (or related), image processing techniques and Proper Orthogonal Decomposition (POD). Sprays were also evaluated using time-resolved x-ray radiography.

Traditional image processing techniques were applied to films over a wide range of conditions and to sprays over a lesser range. Many operating conditions and geometries had dominant frequencies. Generally, dominant frequencies of the same values were observed in both the film and the spray indicating that the atomization behavior of the film translates into the spray. However, a few cases with high dominant frequencies in the film did not have measurable dominant frequencies in the spray. The time-resolved boundary data provided details on the type of nonuniformity being exhibited. A single test geometry and condition, which displayed clear periodic behavior, was selected for additional analysis. The selected spray exhibited asymmetric film behavior a "bouncing" type of spray behavior where the spray centerline periodically departed from the injector centerline. The measured frequency of the bouncing is around 16 Hz.

The POD analysis of this single test case also measured dominant frequencies in the spray and the film of a single test case. These results agreed with the traditional image processing results within the level of uncertainty expected. However, the POD also detected an 880 Hz signal in the film behavior which was not observed in the spray. The general lower energy of this frequency compared to the lower frequency may explain why the 880 Hz signal is not detectable after the evolution and expansion of the spray. The POD results also allow the location and propagation of periodic structures to be visualized. Structures clearly originate in the area of initial liquid-gas contact and widen and elongate as they move downstream in the injector cup.

The time-resolved x-ray radiography, applied to the single spray, again shows the same dominant frequency of the other two techniques. There are time spans with few, small droplets followed by spans of many, large droplets observed from the radiography time traces. The edges of the spray have stronger frequency peaks than the center of the spray. This finding gives some indication of the range of motion of the centerline departures from a mass flux standpoint.

The three different techniques all provide frequency data, but each also provides additional data which the others do not. Film and spray behavior, as examined with tradition processing techniques, provides information on the type and severity of nonuniformity. POD provides visual evidence of periodic structures, their origination and their propagation. Time-resolved x-ray radiography provides details on individual structures and their changes during the nonuniformity. Together, these three techniques complement each other to provide a more detailed picture of spray nonuniformities in Gas-Centered Swirl Coaxial Injectors.

Acknowledgements

A portion of this research was performed at the 7-BM beamline of the Advanced Photon Source, Argonne National Laboratory and was supported by the U.S. Department of Energy, Office of Science, Office of Basic Energy Sciences, under Contract No. DE-AC02-06CH11357. Daniel Duke (Monash University), Chad Eberhart (University of Alabama, Huntsville), Benjamin Halls (Iowa State University), William Miller (Kettering University) and Christopher Powell (Argonne National Laboratory) assisted in the conduction of the x-ray experiments. Benn Eilers (Oregon State University) assisted in the data collection for Proper Orthogonal Decomposition under the American Society for Engineering Education's Air Force Summer Faculty Fellowship program.

References

1. Lightfoot, M.D.A., Schumaker, S.A., Villasmil, L.A. and Danczyk, S.A., *JANNAF 8th Modeling and Simulation, 6th Liquid Propulsion, and 5th Spacecraft Propulsion Joint Subcommittee Meeting*, Huntsville, AL, December 2011.

2. Schumaker, S.A., Danczyk, S.A. and Lightfoot, M.D.A., *47th AIAA Joint Propulsion Conference*, San Diego, CA, July 2011.

3. Lightfoot, M.D.A. and Danczyk, S.A., *11th Triennial International Conference on Liquid Atomization and Spray Systems*, Vail, CO, July 2009.

4. Strakey, P.A., Talley, D.G. and Hutt, J.J., *Journal of Propulsion and Power* 17 (2):404-410 (2001).

5. Schmidt, J.B., Schaefer, Z.D., Meyer, T.R., Roy, S., Danczyk, S.A. and Gord, J.R., *Applied Optics* 48 (4):B137-B144 (2009).

6. Lopez-Pages, E., Dopazo, C. and Fueyo, N., *Journal of Fluid Mechanics* 515 (1-31 (2004).

7. Lightfoot, M.D.A., Danczyk, S.A. and Talley, D.G., *19th Annual Conference on Liquid Atomization and Spray Systems*, Toronto, Ontario, May 2006.

8. Park, J., Huh, K.Y., Li, X. and Renksizbulut, M., *Physics of Fluids* 16 (3):625-632 (2004).

9. Wang, Q., Mondragon, U.M., Brown, C.T. and Mcdonell, V.G., *22nd Annual Conference on Liquid Atomization and Spray Systems*, Cincinnati, OH, May 2010.

10. Carvalho, I.S., Heitor, M.V. and Santos, D., *International Journal of Multiphase Flow* 28 (5):773-789 (2002).

11. Holmes, P., Lumley, J. and Berkooz, G., *Turbulence, Coherent Structures, Dynamical Systems, and Symmetry*, Cambridge University Press, 1996.

12. Krebs, D., Narayanan, V., Liburdy, J.A. and Pence, D.V., *Experimental Thermal and Fluid Science* 34 (4):434-445 (2010).
13. Arienti, M. and Soterious, M.C., *Physics of Fluids* 21 (112104 (2009).
14. Halls, B.R., Heindel, T.J., Meyer, T.R. and Kastengren, A.L., *50th AIAA Aerospace Sciences Meeting*, Nashville, TN, January 2012.
15. Kastengren, A.L., Powell, C.F., Liu, Z., Moon, S., Gao, J., Zhang, X. and Wang, J., *22nd Annual Conference on Liquid Atomization and Spray Systems*, Cincinnati, OH, May 2010.
16. Lin, K.C., Carter, C., Smith, S. and Kastengren, A.L., *50th AIAA Aerospace Sciences Meeting*, Nashville, TN, January 2012, AIAA 2012-0347.
17. Lightfoot, M.D.A., Kastengren, A.L., Schumaker, S.A. and Danczyk, S.A., *24th Annual Conference on Liquid Atomization and Spray Systems*, San Antonio, TX, May 2012.
18. Narayanan, V., Lightfoot, M.D.A., Schumaker, S.A., Danczyk, S.A. and Eilers, B., *23rd Annual Conference on Liquid Atomization and Spray Systems*, Ventura, CA, May 2011.
19. Otsu, N., *IEEE Transactions on Systems, Man, and Cybernetics* 9 (1):62-66 (1979).
20. Matlab R2008b, MathWorks Inc., 2008.
21. Berger, M.J., Hubbell, J.H., Seltzer, S.M., Chang, J., J.S., C., Sukumar, R., Zucker, D.S. and Olsen, K., *XCOM: Photon Cross Sections Database, NIST Standard Reference Database 8 (XGAM)*, http://www.nist.gov/pml/data/xcom/index.cfm. , 2012.